Quantum dots formed in a GaAs / AlGaAs quantum ring

A. Mühle, W. Wegscheider, and R. J. Haug

Citation: Appl. Phys. Lett. **92**, 013126 (2008); doi: 10.1063/1.2833694
View online: https://doi.org/10.1063/1.2833694
View Table of Contents: http://aip.scitation.org/toc/apl/92/1
Published by the American Institute of Physics

Quantum dots formed in a GaAs/AlGaAs quantum ring

A. Mühle[a)]
Institut für Festkörperphysik, Leibniz Universität Hannover, Appelstraße 2, 30167 Hannover, Germany

W. Wegscheider
Institut für Angewandte und Experimentelle Physik II, Universität Regensburg, Universitätsstraße 31, 93040 Regensburg, Germany

R. J. Haug
Institut für Festkörperphysik, Leibniz Universität Hannover, Appelstraße 2, 30167 Hannover, Germany

(Received 19 November 2007; accepted 19 December 2007; published online 10 January 2008)

We demonstrate the tunability of a GaAs/AlGaAs quantum ring showing coherent Aharonov-Bohm oscillations up to a gate voltage regime where the ring splits into three quantum dots. This is explained based on the structure's special confinement potential. We characterized the dots by analyzing the corresponding sets of Coulomb blockade lines. Additionally, the spatial configuration of the dots was confirmed by charge measurements using an adjacent quantum point contact.
 [DOI: 10.1063/1.2833694]

The investigation of semiconductor quantum rings has been a growing field of interest in recent years. Notably, their use as phase detectors proved to be an important application. For example, the phase shift of an electron traversing a quantum dot could be measured by using a dot embedded in the arm of a quantum ring interferometer.[1,2] The area of research on multiple quantum dots also advances significantly. Except for basic experiments in the mid-90s,[3,4] only recently, a few groups were able to study coupled triple dots.[5–8]

In this paper, we report on the formation of three quantum dots inside a quantum ring due to the special shape of the confinement potential. This leads to the perspective of deliberately forming embedded multidots by only small manipulations in the constrictions of a ring.

Our device was fabricated from a GaAs/AlGaAs heterostructure consisting of 5 nm GaAs as a cap layer, 6.5 nm AlGaAs, 2 nm AlAs, 2 nm GaAs, a Si-δ layer, an AlGaAs barrier which is 18.5 nm wide and 1 μm GaAs (from top to bottom). A resulting two-dimensional electron gas (2DEG) is located 34 nm below the surface with an electron density of $n_e = 3.91 \times 10^{15}$ m^{-2} and a mobility of $\mu_e = 64.3$ m^2 V^{-1} s^{-1}. A quantum ring with adjacent quantum point contact (QPC) was formed using the method of local anodic oxidation with an atomic force microscope (AFM).[9–12] This technique allows to create insulating lines cutting through the 2DEG by writing oxide lines on the surface of the sample.

An AFM image of our device is shown in the inset in Fig. 1. It consists of a ring with an outer diameter of 360 nm surrounding an oxide dot with a diameter of 100 nm. The ring is connected to two leads, source (S) and drain (D), via point contacts with a width of 100 nm. Next to one arm of the ring, a 100 nm quantum point contact is located with its own source and drain leads (source S_{QPC} and drain D_{QPC}). This external QPC acts as a charge detector since its effective width is sensitive to the electrical field of the ring's electrons. Two areas insulated from the rest of the structure serve as gates (G1 and G2) and can be used to tune the other parts of the device.

In order to obtain a more complex system, the oxide forming the center of the ring is positioned asymmetrically leaving more space in the upper part of the ring while it is shifted into the lower arm. Therefore, it forms a sort of constriction in the lower arm. Thus, the conducting region of the ring is roughly divided into one island in the upper arm and two smaller islands left and right of the constriction in the lower arm. These three segments are expected to be separable by appropriate gate voltages.

The experiments we present in this paper were done using standard lock-in technique in a two-point measurement setup connected to the source and drain contacts. The resistance of the leads can be neglected here, since it never exceeds a few kilo-ohms, while our structure with tunneling barriers on both sides has a total resistance of at least several hundred kilo-ohms up to some megaohms, depending on the gate voltage. The sample was mounted in a dilution refrigerator at a base temperature of $T = 20$ mK.

Most measurements on the device were done without the external QPC. Instead, the areas of S_{QPC}, D_{QPC}, and G1 were combined to form one large gate QPC+G1.

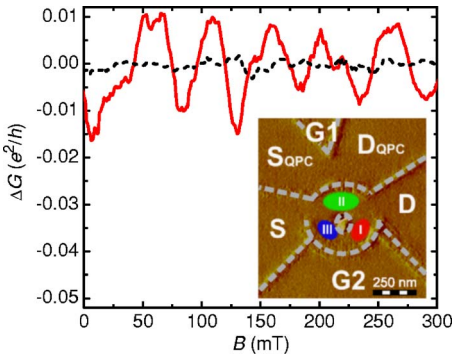

FIG. 1. (Color online) Difference ΔG between the conductance G and the nonoscillating background as a function of B for $V_{QPC+G1} = 140$ mV, $V_{G2} = 145$ mV (straight line) and $V_{QPC+G1} = 30$ mV, $V_{G2} = 100$ mV (dashed line). The Aharonov-Bohm oscillations with a period of 51 mT are clearly visible in the first situation but vanish in the other one. Inset: an atomic force microscope image of the device. The quantum dots that formed in the structure are marked. The middle of the oxide lines is traced in grey for clarity. The areas labeled S_{QPC}, D_{QPC}, and G1 can be combined and used as one single gate QPC+G1.

[a)]Electronic mail: amuehle@nano.uni-hannover.de.

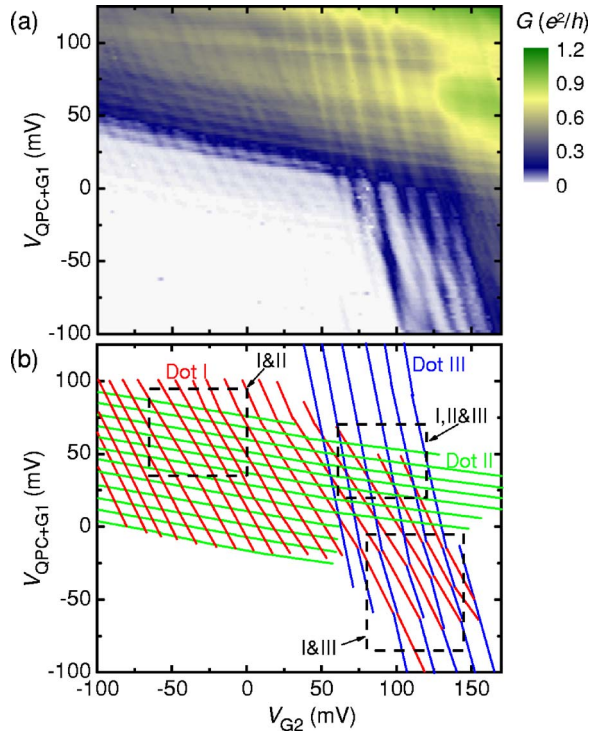

FIG. 2. (Color online) (a) The conductance G through the quantum ring in dependence of the applied gate voltages. (b) The positions of the Coulomb blockade lines visible in the spectrum shown in (a). The dashed boxes mark the regions corresponding to the depictions in Fig. 3. They are labeled with the numbers of the dots whose lines cross inside of their area. Each set of lines is labeled with respect to the corresponding quantum dot.

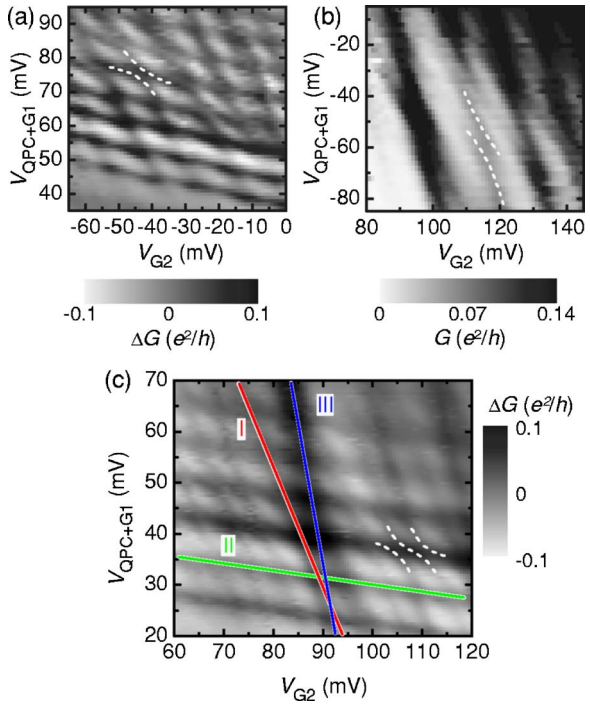

FIG. 3. (Color online) (a) A section of the conductance plot where the Coulomb lines of dots I and II cross each other. To emphasize the features, only the difference ΔG from the background is shown. One of the anticrossings is traced. (b) Part of the region where the blockade lines of dots II and III meet. One anticrossing is marked. (c) Part of the region where the blockade lines of all three dots meet. Here, again, a background has been removed. For each dot, one line is marked and labeled. Additionally, one of the crossing patterns indicating the presence of triple dot physics is traced.

Since we started from a ringlike geometry, we expect to see the Aharonov-Bohm oscillations. This is indeed observed for a certain gate voltage regime. The results from measuring electronic transport through the ring in dependence of an externally applied magnetic field B are shown in Fig. 1 for two different gate configurations. To enhance the oscillations in the differential conductance G, a background was subtracted from the raw data leaving the difference ΔG with only the oscillatory part of the signal. To obtain that background, the original curves were smoothed by boxcar averaging using adequately wide intervals. It can be seen that for larger positive gate voltages, Aharonov-Bohm oscillations are visible (solid line). Their amplitude of $0.02e^2/h$ corresponds to a visibility of 1.5% relative to the removed background of about $1.3e^2/h$. Their periodicity of ΔB=51 mT implies a diameter of 321 nm for the electronic path through the ring which fits perfectly to the written geometry. Applying smaller gate voltages eventually results in a vanishing of the Aharonov-Bohm effect. This is also depicted in Fig. 1 (dashed line). This observation shows that lower gate voltages lead to a regime where coherent transport through the ring is disrupted. Thus, it is consistent with the assumption that the ring can be divided into separated segments.

The transport spectrum that develops when the gate voltages are swept without a magnetic field B is depicted in Fig. 2(a). The conductance G through the ring is plotted in dependence of the applied gate voltages over the ranges of $-100\ \text{mV} \leqslant V_{\text{QPC+G1}} \leqslant 125\ \text{mV}$ and $-100\ \text{mV} \leqslant V_{\text{G2}} \leqslant 170\ \text{mV}$. The lower left region of the figure shows the regime in which the negative gate voltages effectively close the connections between the ring and the leads and therefore the conductance vanishes. The highest transmission through the device can be seen in the upper right corner at the largest positive gate voltages. Between these regions, the constrictions to source and drain are tuned to form thin tunneling barriers and Coulomb blockade lines are visible. In Fig. 2(b), a scheme of the Coulomb lines' positions over the observed voltage region is drawn. It is clearly visible that each line belongs to one of three distinct groups, showing the existence of three different quantum dots in the structure. These dots are referred to as I, II, and III and the lines are labeled accordingly. Measurements depending on a source-drain voltage for each set of lines led to the observation of Coulomb diamonds, confirming the nature of the blockade lines.

In the transport spectrum, the blockade lines of dot II cross the lines of dot I with only slight interaction. In contrast, the Coulomb lines belonging to dot I and those of dot III show notable anticrossings where they meet in the lower right quarter of the conductance plot. This indicates that dot I is coupled stronger to dot III than to dot II. In both cases, the rounded shape of the lines at the triple points suggest tunnel coupling to be present. There is no region in the plot where crossings between the lines originating from dot II and those of dot III can be observed without the presence of also the lines of dot I.

The sections of the plot where anticrossings are present are marked in Fig. 2 and shown in more detail in Fig. 3. In Fig. 3(a), it can be seen that the interaction of dots I and II is more discernible for larger $V_{\text{QPC+G1}}$ and smaller V_{G2}. This fits to the expectation that such tuning shifts dot I closer to the upper part of the ring while dot II cannot retreat. In Fig. 3(b), anticrossings between the lines of dots I and III are shown. Figure 3(c) depicts the region where all three types of block-

ade lines meet and complex patterns of anticrossings appear. Here, the so-called quadruple points occur.[6] This indicates tunnel coupling between all three dots and thus the formation of a real triple dot in this regime.

Analyzing the distances of the Coulomb blockade lines in the transport spectrum, the capacitances between the different quantum dots and each of the two gate areas QPC+G1 and G2 can be obtained. For dot I, these values are $C_{\mathrm{QPC+G1,I}}=6.7$ aF and $C_{\mathrm{G2,I}}=12.5$ aF, for dot II, they are $C_{\mathrm{QPC+G1,II}}=20.9$ aF and $C_{\mathrm{G2,II}}=3.7$ aF, and for dot III, $C_{\mathrm{QPC+G1,III}}=2.3$ aF and $C_{\mathrm{G2,III}}=11.9$ aF. Since these capacitances can be used as a measure for the coupling of each dot to the different gate areas, it can be derived that dots I and III are positioned closer to G2 than to QPC+G1. For dot II, it is considered as being reverse.

Additionally, by using the aforementioned additional Coulomb diamond measurement, the charging energies of the dots and their capacitances toward the source contact can be calculated. This yields the charging energies $E_{\mathrm{char,I}}=3.1$ meV, $E_{\mathrm{char,II}}=2.1$ meV, and $E_{\mathrm{char,III}}=3.6$ meV while the source capacitances are $C_{\mathrm{I,S}}=23.9$ aF, $C_{\mathrm{II,S}}=49.3$ aF, and $C_{\mathrm{III,S}}=35.7$ aF. Since the charging energies and the ring's geometry suggest a similar size for dots I and III, their capacitances to source may be compared. Thus, dot III is found to be located closer to the source area than dot I.

The positions emerging from these calculations are marked in the inset in Fig. 1 by the ellipses drawn into the arms of the ring. It can be seen that they fit exactly to the geometric shape of the lithographic structure with one dot in the upper part and the two other ones on both sides of the constriction in the lower arm.

To further investigate the situation on the ring, measurements of the transport through the QPC were performed. In this setup, the leads connected to the QPC were no longer utilized as parts of a gate area and only G1 and G2 were used to tune the structure. Kinks in the signal of a QPC capacitively coupled to a quantum dot result from charging of the dot.[13] This is due to the gatelike influence of the dot's charge on the effective width of the constriction forming the QPC. The measurement of the QPC's conductance and the transport through the ring may be compared for $V_{\mathrm{G1}}=0$ mV and $V_{\mathrm{QPC+G1}}=0$ mV, respectively. There, the changes of charge observed with the QPC match the Coulomb lines of dot II. Although in the spectrum of the ring other blockade lines can be seen in the corresponding region, no further features are visible in the QPC signal. Thus, it is only dot II which has an influence on the QPC. This is an independent confirmation of our finding that dot II is adjacent to the QPC while the other two dots I and III are located on the opposite side of the ring.

In conclusion, we measured transport through an asymmetric quantum ring in dependence of external gate voltages. The observed Coulomb blockade lines show the existence of three distinct quantum dots inside the ring. Anticrossings of these lines indicate tunnel coupling between the dots. In dependence of the gate voltage, two regimes with double dots as well as one with a real triple dot are accessible. Calculation of the dots' capacitances toward the outer parts of the structure are used to determine the dots' positions. Additional measurements using the quantum point contact next to the ring as a charge detector on these quantum dots confirm the findings about these locations. Comparison with the lithographic structure of the device verifies that the spatial arrangement of the dots originates from the small asymmetry of the oxide dot in the center. Thus, we demonstrate the generation of a complex quantum structure from a simpler design by only a minimal variation in the geometry.

We acknowledge financial support by BMBF via nanoQUIT.

[1] R. Schuster, E. Buks, M. Heiblum, D. Mahalu, V. Umansky, and H. Shtrikman, Nature (London) **385**, 417 (1997).
[2] M. Sigrist, A. Fuhrer, T. Ihn, K. Ensslin, S. E. Ulloa, W. Wegscheider, and M. Bichler, Phys. Rev. Lett. **93**, 066802 (2004).
[3] R. J. Haug, Electrochim. Acta **40**, 1283 (1995).
[4] F. R. Waugh, M. J. Berry, D. J. Mar, R. M. Westervelt, K. L. Campman, and A. C. Gossard, Phys. Rev. Lett. **75**, 705 (1995).
[5] A. Vidan, R. M. Westervelt, M. Stopa, M. Hanson, and A. C. Gossard, Appl. Phys. Lett. **85**, 3602 (2004).
[6] L. Gaudreau, S. A. Studenikin, A. S. Sachrajda, P. Zawadzki, A. Kam, J. Lapointe, M. Korkusinski, and P. Hawrylak, Phys. Rev. Lett. **97**, 036807 (2006).
[7] D. Schroer, A. D. Greentree, L. Gaudreau, K. Eberl, L. C. L. Hollenberg, J. P. Kotthaus, and S. Ludwig, Phys. Rev. B **76**, 075306 (2007).
[8] M. C. Rogge and R. J. Haug, e-print arXiv:0707.2058v3.
[9] M. Ishii and K. Matsumoto, Jpn. J. Appl. Phys., Part 1 **34**, 1329 (1995).
[10] A. Fuhrer, S. Lüscher, T. Ihn, T. Heinzel, K. Ensslin, W. Wegscheider, and M. Bichler, Nature (London) **413**, 822 (2001).
[11] U. F. Keyser, C. Fühner, S. Borck, R. J. Haug, M. Bichler, G. Abstreiter, and W. Wegscheider, Phys. Rev. Lett. **90**, 196601 (2003).
[12] R. Nemutudi, M. Kataoka, C. J. B. Ford, N. J. Appleyard, M. Pepper, D. A. Ritchie, and G. A. C. Jones, J. Appl. Phys. **95**, 2557 (2004).
[13] M. Field, C. G. Smith, M. Pepper, D. A. Ritchie, J. E. F. Frost, G. A. C. Jones, and D. G. Hasko, Phys. Rev. Lett. **70**, 1311 (1993).